We are IntechOpen, the world's leading publisher of Open Access books Built by scientists, for scientists

6,900
Open access books available

185,000
International authors and editors

200M
Downloads

Our authors are among the

154
Countries delivered to

TOP 1%
most cited scientists

12.2%
Contributors from top 500 universities



WEB OF SCIENCE™

Selection of our books indexed in the Book Citation Index in Web of Science™ Core Collection (BKCI)

Interested in publishing with us?
Contact book.department@intechopen.com

Numbers displayed above are based on latest data collected.
For more information visit www.intechopen.com



Chapter 5

Vertical Natural Vibration Modes of Ballasted Railway Track

Akira Aikawa

Additional information is available at the end of the chapter

http://dx.doi.org/10.5772/intechopen.79738

Abstract

Impact loads from running trains induce natural vibration within the ballast layer, which causes ballast deterioration over time. This study measured the natural vibration characteristics of the ballast layer using field measurements, full-scale impact loading experiments and large-scale finite element analysis. Experimental test results indicate that the vibration components in the high-frequency range are dominant in ballast responses under loading and that ballast motions during unloading are mainly induced by vibration components in the low-frequency range, causing large displacement over a long duration. Numerical results indicate that the normal frequency of the vertical elastic vibration mode is detected at approximately 310 Hz and that the rigid-body bounce mode of the ballast layer occurs at one-third of the elastic vibration mode frequency. They coincide substantially with values held by field measurements. Stress acting on the angular part of the ballast is more than 1000 times greater than the average loading stress under the sleeper bottom. The combined structure, which consists of the ballast layer and sleepers, vibrates easily in synchrony with resonance motions induced by the impulse waves. Improvement of the contact condition on the sleeper bottom is expected to decrease the displacement amplitude of ballast gravel, thereby reducing ballast degradation.

Keywords: impact loads, natural vibration of granular layer, full-scale impact loading experiments, tensionless analysis

1. Introduction

A ballasted track is characterized by its structure, with a ballast layer sandwiched between sleepers and a roadbed, which greatly reduces impact loads generated by dynamic rolling—contact interaction between the wheels and rails. However, this benefit has an adverse effect:

IntechOpen

© 2018 The Author(s). Licensee IntechOpen. This chapter is distributed under the terms of the Creative Commons Attribution License (http://creativecommons.org/licenses/by/3.0), which permits unrestricted use, distribution, and reproduction in any medium, provided the original work is properly cited. CC BY

The ballasted tracks are structurally prone to deteriorate over time. They absolutely require periodic maintenance work and repair. Recently, many attempts were made to improve the ballasted track structure. For example, many types of elastic and/or viscoelastic structural members, such as rail pads, under-sleeper pads and under-ballast mats, were attempted to reduce ballast degradation [1–3]. In one experimental investigation, the sleeper's vibration characteristics, including the dynamic effects of sleeper/ballast interactions, were investigated through a modal analysis to predict the railway track's dynamic response [4]. Dynamic wheel/rail interactions, which significantly contribute to impact vibration and noise, were also investigated for rail and wheel surface defects in field measurements and numerical simulations [5–8]. When considering the future of the railway management, it is impossible to disregard the necessity for frequent maintenance that is dependent upon manual aid. Therefore, the need exists to improve maintenance methods for the ballasted track based on findings from empirical and numerical investigations of the dynamic response characteristics and deterioration factors of the ballast layer.

Running trains cause dynamic loads mainly through two mechanisms [9, 10]. One is the dynamic load from passing axle loads as a train passes. The related frequency characteristics, which depend on the number of axles passing per unit of time, are limited to low frequencies of only several Hertz to approximately 30 Hz. The other mechanism is the impact load that is generated dynamically by the rolling contact mechanism between the wheels and rails. The ballast layer transmits this sharp pulse-shaped impact load superimposed on the low-frequency loads from passing axles. This waveform, when transformed into a frequency domain, exhibits numerous vibration components with broadband characteristics that extend from low frequencies to several kilohertz. That is to say, dynamic response measurements of the ballasted track require high-precision measurements of vibration components ranging broadly from several Hertz to several kilohertz. Outputs of sensor would be degraded by noise of tens of millivolts deriving from the inductive currents of high-voltage overhead cables in conventional field measurements, which necessitated the use of a low-pass filter to alleviate that interference. Ensuring the measurement accuracy of high-frequency vibration components exceeding 50–100 Hz was impossible under such conditions. For that reason, no comprehensive discussion of these components has been reported in the literature to date.

This chapter gives accurate field measurements of the dynamic responses of the ballasted track with a train passage at a sampling frequency of 10 kHz without low-pass filters, using special sensing sleepers and sensing stones produced by the authors [11, 12]. Using the measurement effects, the analysis can be done with a focal point on propagation characteristics of dynamic loads inside the ballast layer and vertical natural modes of the ballast layer. Moreover, the author conducted a free fall-weight impact loading test on a full-scale mock-up of a ballasted track to ascertain the response motions of the ballast layer, with high rapidity and with high accuracy, in the high-frequency region immediately after the impact load was used [13]. Furthermore, using a direct solver MUMPS [14–17] corresponding to large-scale parallel computing of a distributed memory type, according to finite element transient response analysis FrontISTR [18] and Advance/FrontSTR [19] based on a fine ballast aggregate model, both the elastic natural vibration mode and the rigid-body bounce natural vibration mode of the granular ballasted layer are simulated numerically.

http://dx.doi.org/10.5772/intechopen.79738

2. Rigid-body bounce vibration mode and elastic natural vibration mode

In general, a dynamic load propagates as an elastic wave through the interior of an object, consequently inducing the natural vibration modes specific to the object, which can be applied to the ballasted track composed of the ballast aggregate. Although the ballast layer is a discontinuous structure, it presumably has natural vibration modes that are specific to the ballasted track. **Figure 1** shows some characteristics of the principal natural vibratory motions in the vertical direction of the ballast layer [20]. One characteristic is the rigid-body bounce natural vibration mode. Another is the elastic shrinkage natural vibration mode. The ballasted track structure represents a single degree of freedom system that includes sleepers, rails and other components which constitute the track structure mass, along with the ballast layer and roadbed which constitute the spring rigidity component. In the bounce natural vibration mode, this single degree of freedom system moves vertically and rigidly under a train's dynamic load. The ballast layer acts as an elastic one-directional spring in the vertical direction. Rigid-body natural vibration modes of six kinds exist: They are translational and rotational along each of the three axes. In both the dynamic loads applied to the ballast layer and in the responses of the ballast layer, the translational vibration components in the vertical direction are predominant.

Therefore, this research specifically examines the translational bounce behaviour in the vertical direction. According to the dynamics, the natural frequency of the first-order rigid-body bounce mode f_1 is given theoretically as $f_1 = \sqrt{k/m}/(2\pi)$, where k and m, respectively, denote the ballast stiffness and overburden mass of the track structure. This mode reportedly exists at approx. 100 Hz [21].

The elastic vibration mode is the motion by which the whole ballast layer shrinks and stretches vertically as an elastic body. This natural vibration mode is considered not to occur in a normal-state ballast layer but to occur when the ballast layer is under high confining pressure generated by the train's weight applied to the layer. To date, no report of the relevant literature has described a study conducted to capture this mode, that is, ballast motion in the frequency domain related to this mode. Moreover, on a real track, natural vibration that

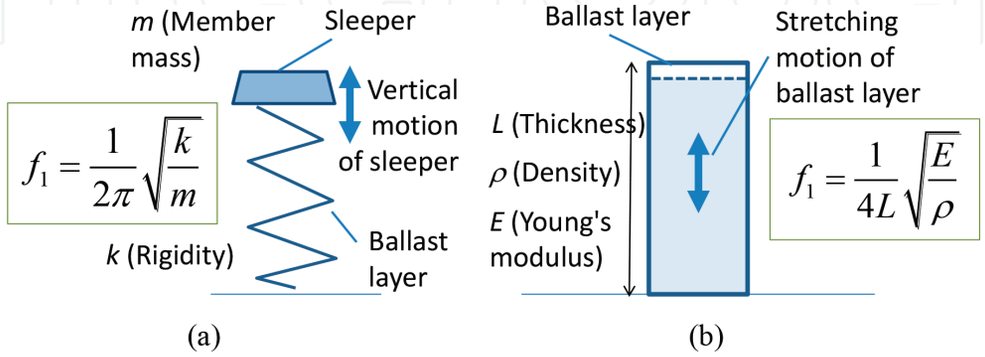


Figure 1. Principal vertical natural vibration motions of the ballast layer. (a) Rigid-body bounce mode, (b) elastic shrinkage mode.

entails bending deformation and torsional deformation of the members occurs. According to the physical theory related to standing waves on the railway track, the natural frequency of the elastic first-order vibration mode f_1 is given theoretically as $f_1 = \sqrt{(E/\rho)}/(4L)$, where E, ρ and L, respectively, denote the ballast layer's Young's modulus, density and thickness.

3. Vibration tests by the use of a full-scale mock-up

The author built a full-scale mock-up of the ballasted track structure and investigated natural vibration characteristics of the ballasted track by performing an experimental modal analysis based on impulse excitation tests.

Figure 2 shows the profile/plane of the mock-up and the sensor positions [22–24]. To build the full-scale mock-up, the author employed new ballast using hard andesite, which complies with the same standard for the real track. They were compacted sufficiently. Type 3 prestressed concrete (PC) monoblock sleepers were used for the mock-up. They are used widely for the metre-gauge (1067 mm-wide) railway lines that are conventionally used for Japan Railway Companies. For the prevention of interference of vibration effects of the concrete frame, urethane foam panels were sandwiched between the mock-up and the outer concrete frame. The author installed acceleration sensors on the mock-up and the concrete frame, vibrated the mock-up and ensured that the vibrations were sufficiently isolated to assess the vibration-insulating properties. The author conducted tests by hitting the end of the sleeper laterally, longitudinally and vertically with an impulse hammer to make it vibrate. Test records included measurements of the acceleration responses: 22 sleeper locations and several ballast layer locations. From those data the accelerance was calculated: the transfer functions of the acceleration responses to the excitation force in the frequency domain. Then

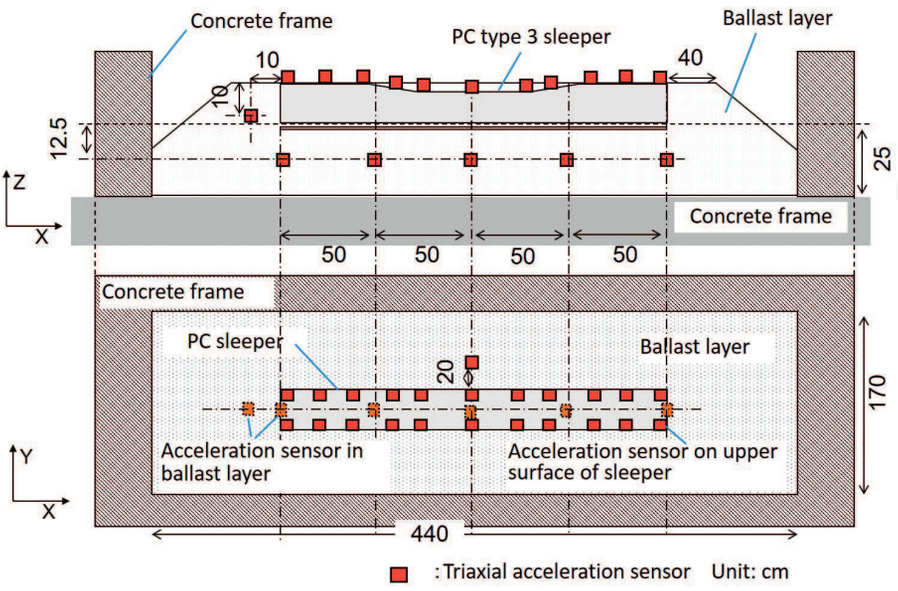


Figure 2. Overview of full-scale vibration test.

http://dx.doi.org/10.5772/intechopen.79738

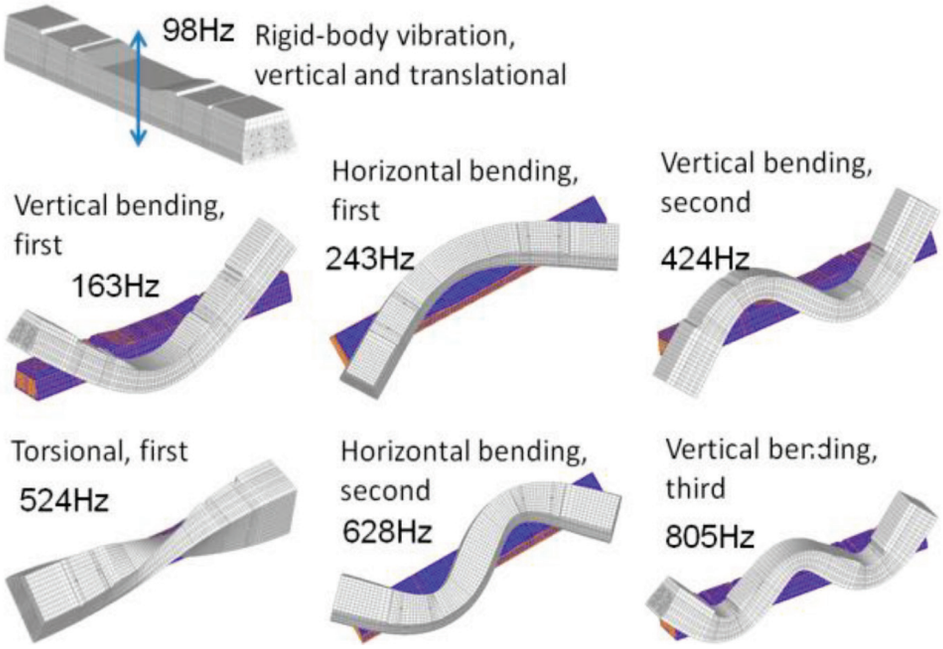


Figure 3. Mode shapes of natural vibration acquired from test results.

experimental modal analysis was conducted considering the location relations of the measuring points. As a result, for the ballasted track, the author was able to identify the natural vibration frequencies and their modal shapes between the low-frequency domain and 1 kHz.

Figure 3 presents the natural vibration frequencies and the specific modal shapes of the ballasted track that were acquired from the test results [22–24]. Although there are rigid-body vibration modes of six types as described above, the figure shows only the rigid-body translational mode in the vertical direction. It also shows that the vertical and translational rigid-body vibration is generated at 98 Hz, which agrees well with earlier reported research results. Furthermore, six types of dominant natural vibration mode entailing the bending and torsional deformations of sleepers are identified as shown in the same figure. Nevertheless, the author was unable to capture any vertical elastic natural vibration mode of the ballast layer in this test. That is true probably because the elastic vibration modes of the whole ballast layer would occur only when the ballast layer continuity is sufficiently satisfied according to the train loads on the ballast layer.

4. Field measurements and spectral analysis

Dynamic responses were measured on an actual ballasted track of a main conventional railway line in Japan to identify the dominant natural vibration modes of the ballasted track. The track structure at the measurement site, consisting of continuous welded rail weighing 60 kg/m and type 3 PC sleepers, was designed based on the Japanese standard [25], which allows a running speed higher than 130 km/h. The measurement site was located on a solid embankment in a straight section. For spacing between the sleepers, 41–42 sleepers are positioned over a

distance of 25 m. The author chose a straight section with satisfied track conditions, based on measurement data from an inspection car. The ballast layer at the measurement site is made of new andesite hard stones with clear-cut edges. The ballast layer is approx. 30 cm thick.

Figure 4 presents an overview of sensor positions. Details of the measurements are described in earlier reports of the literature [26, 27]. This article specifically examines the measured responses for a passenger train moving at approx. 120 km/h (sampling frequency is 10 kHz). The sleeper vibration acceleration and the ballast vibration acceleration were measured using piezoelectric triaxial acceleration sensors: 10 mV/G sensitivity, 500 G measurement range and 2–10,000 Hz frequency range within 5% deviation. The ratio of noise to the maximum measurable acceleration is approximately 0.002%. The acceleration sensor also offers an appropriate level of performance to enable measurement for the determination of load characteristics in a high-frequency domain. The following analyses were conducted by obtaining linear amplitude spectra by application of fast Fourier transformation of the time history response waveforms in response to vibration accelerations, with smoothing at a 20 Hz bandwidth.

Figure 5 shows a special sensing sleeper designed to assess the dynamic load distribution on the sleeper bottom, for a wide frequency range from a low frequency of 0.01 Hz up to a high frequency of several tens of kilohertz. The sensing unit comprises a type 3 PC sleeper fitted with many ultra-thin-type impact load sensors. Attached to the sleeper's whole undersurface is a solid mass comprising 75 impact load sensors (25 pieces × 3 rows). Each impact load sensor has a main body and cover members. The main body including a piezoelectric film has solid cover plates on both surfaces. The cover plates (8 cm × 8 cm) transmit impact load to the main body in cases of impact loads of a running train, thereby preventing sensor breakage [12, 27]. Each sensor can measure a load up to a maximum of 10 kN. The sensor has thin metal plates attached to both sides of a thin piezo-film. The structure, which resembles that of a condenser, has no internal resistance. For that reason, no current is induced by noise sources, even in the electromagnetically high-tension environment that prevails during train operation. This

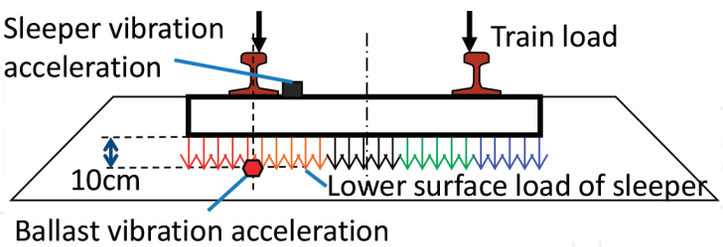


Figure 4. Measuring sensor positions.

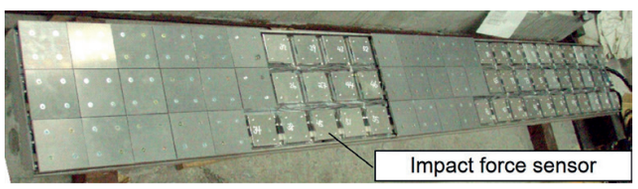


Figure 5. Overview of sensing sleeper.

feature enables high-quality load measurement. Both terminals output a charge that is proportional to the impact load, but digitization of the charge output is extremely difficult. For that reason, the charge from the sensor is usually converted into a voltage by integrating the electric circuit attached to a sensor output terminal (charge amplifier). For that purpose, an impedance transformation circuit with extra-high impedance, ultra-low noise and differential input-type operational amplifiers (OP-amps) can be used for the instrumentation preamplifier. Moreover, this sensor has good reactivity. Because the output voltage can be as high as several tens of volts, the ratio of noise to the maximum measuring load is as low as 0.003%. The sensor can measure load characteristics at high frequencies.

Figure 6 shows the acceleration amplitude spectrum and the displacement amplitude spectrum of the ballast gravel at 10 cm depth. The acceleration spectrum shows that components at frequencies higher than 100 Hz as well as the low-frequency components contribute greatly to the ballast response. These high-frequency vibration components are attributable to the sharp pulse-shaped impact loads induced by the dynamic mechanisms between the wheels and rails.

When particularly addressing the ballast displacement, its amplitude is extremely small in the high-frequency domain. For instance, the displacement amplitude is only 1/1000 μm at a frequency of approx. 800 Hz, which is equivalent to the natural frequency of the ballasted track entailing the third mode of the vertical bending of the sleeper. Therefore, the vibration components in the high-frequency domain are not transmitted by rigid-body vibrations around the centre of gravity of the ballast gravel, but the dynamic loads are transmitted through the elastic undulation propagation because of the local and minute deformation behaviour and sliding behaviour at the tips of the edges of contact points between the ballast stones. However, the displacement amplitude in the low-frequency domain from several Hertz to 20 Hz is several thousand times higher than those in the high-frequency domain. Consequently, the loads in the low-frequency domain are transmitted mainly through rotational and translational rigid-body vibrations of the individual ballast gravel particles. This figure also depicts peak profiles of responses related to the natural vibration modes of the

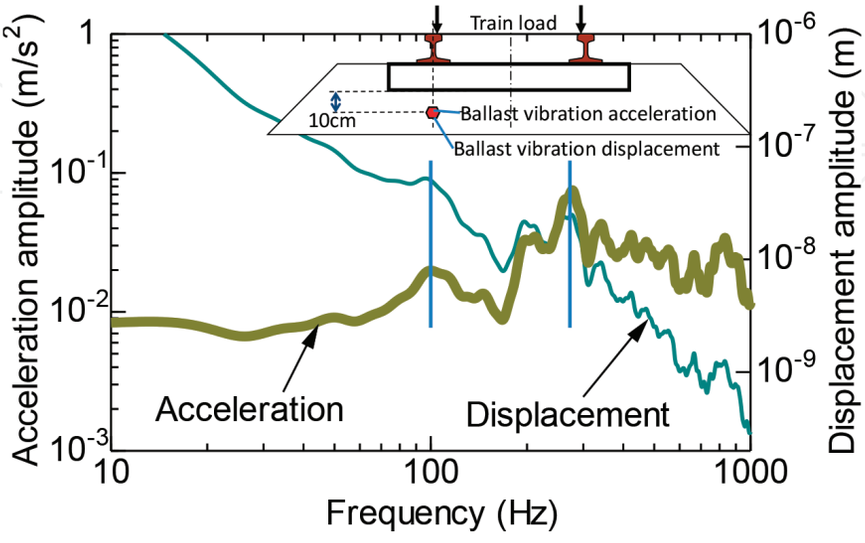


Figure 6. Acceleration and displacement amplitude spectra of the ballast (measured).

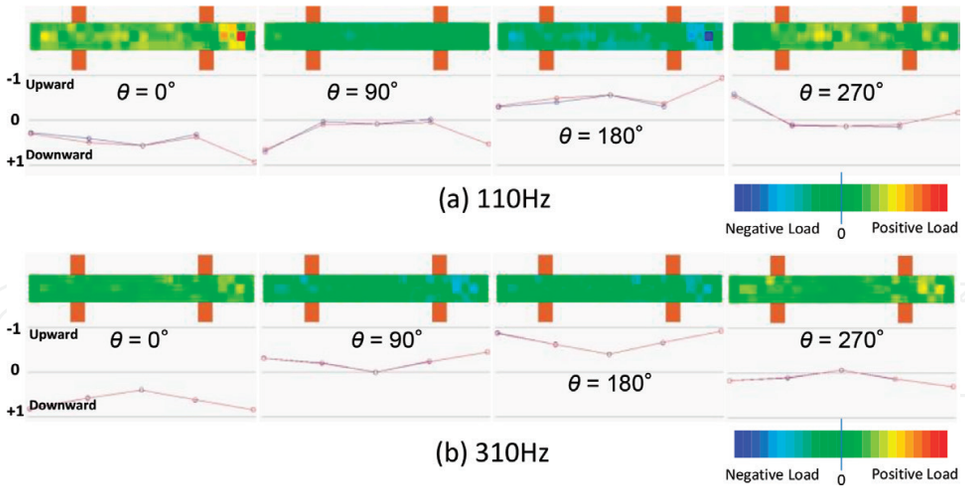


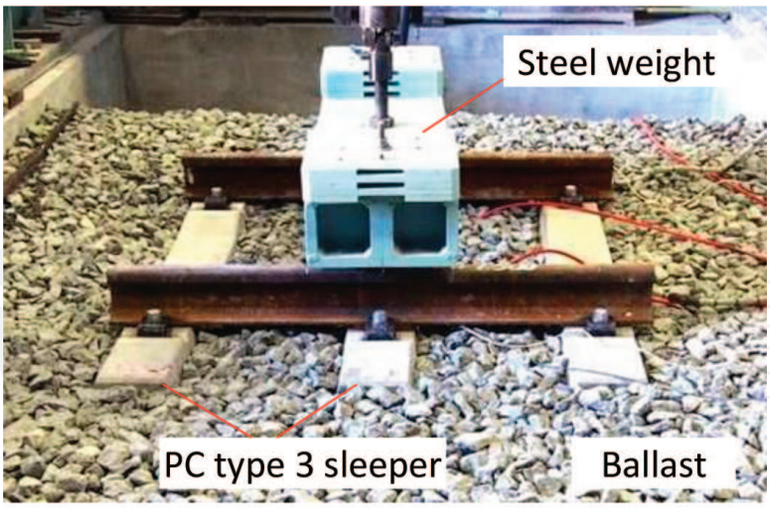
Figure 7. Distribution of vertical loading at the bottom of the sensing sleeper and normalized displacement at the top of the sleeper (measured).

ballasted track explained in the preceding paragraph. These curves identify the rigid-body resonance mode of the ballast layer around 100 Hz and indicate another large peak profile at around 300 Hz. From the full-scale experiment presented in **Figure 3**, the rigid-body natural vibration mode of the ballasted track appears at 98 Hz.

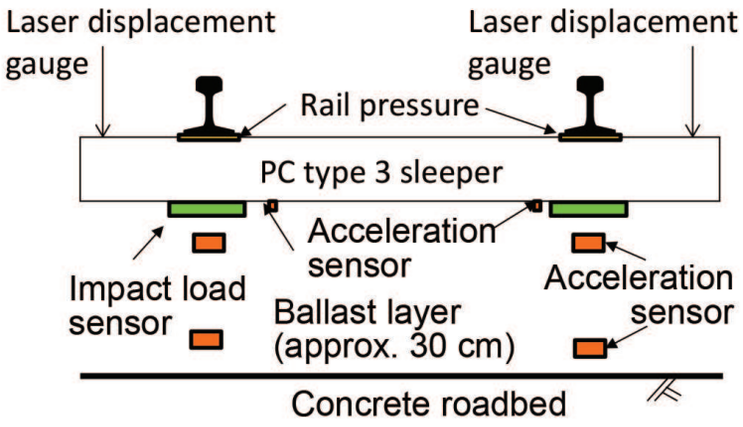
Figure 7 shows the relation between the two-dimensional distribution of the vertical loading on the bottom surface of the sleeper and the normalized vertical displacement of the sleeper in cases of two frequencies (110 and 310 Hz), which give the peak profiles of the response curves. In the figures, θ denotes the relative phase angles with reference to vertical motion at the centre of the sleeper. In the distribution maps, red denotes the positive load (compression). Blue shows the negative load (tension). Regarding the sleeper motion, the downward direction indicates the downward behaviour of the sleeper. The upward direction indicates the upward behaviour of the sleeper. Panels (a) and (b) show that the sleeper repeats a vertical periodic movement at these frequencies, entailing bending deformation of the sleeper at high frequencies, in synchronization with the phase angles.

5. Drop-weight impact loading test

The author repeatedly performed drop-weight impact loading tests using a full-scale mock-up of the ballasted track, dropping a steel weight from a given height and applying impact loads having a sharp pulse shape directly to the track structure. **Figure 8(a)** presents an overview of the test device. **Figure 8(b)** depicts the positions of sensors used for the measurements. The test setup consists of a 30 cm-thick ballast layer built with new andesite ballast gravel on a concrete roadbed. A track structure was built using three pieces of type 3 PC sleepers and two pieces of rails weighing 60 kg/m. The steel weight frame, positioned over the sleeper at the centre, was dropped repeatedly from the given height to apply impact loads to the track structure. Measured data for the magnitude of the impact loads, the vertical displacement of



(a)



(b)

Figure 8. Overview of impact loading test. (a) Drop-weight impact test device, (b) sensor positions.

the sleepers and the acceleration responses of sleepers and ballast were recorded by sampling the data at 10 kHz or 20 kHz. This chapter presents a discussion of the measurement results of the displacement responses of the sleepers [9, 13].

Figure 9(a) shows the time history response of the centre sleeper's vertical displacement after impact loading. This average curve shows results obtained from about 4000 loading tests, excluding initial loading of the first 1000 iterations. The downward displacement in the chart shows the ballast layer compression. The upward displacement represents extension of the ballast layer. **Figure 9(b)** especially depicts data obtained at the moment immediately after loading. The average value of the impact load on the ballast through the left and right rails was 217 kN. The figure shows that because of the compression applied by an impact load, the ballast layer instantaneously deforms elastically. The compression produces maximum downward displacement of 0.178 mm in 0.71 ms. Subsequently, it returns to the preloading

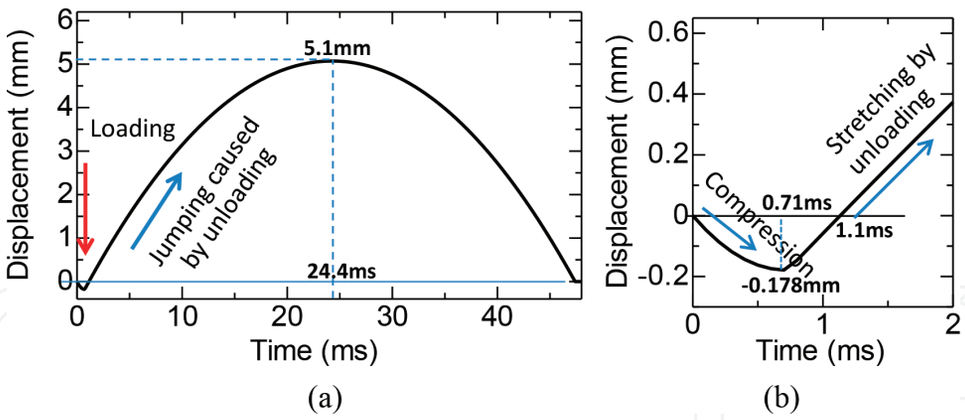


Figure 9. Vertical displacement of sleepers immediately after impact loading. (a) Sleeper displacement, (b) close-up of displacement.

position in 1.1 ms. Results show that only about 1 ms is necessary for the ballast layer compression and restoration. Displacement responses of the sleeper and load during that time include few vibration components at low frequencies.

Following the compression and restoration motions of the ballast layer, sleeper-jumping occurs. The average jumping speed is approximately 1.71 times as high as the average of the compression speed. Their initial speed can be approximately 12.1 times faster than the average compression speed. The jumping height of the sleeper reaches 5.1 mm in 24.4 ms. The sleeper returns to the initial position within 46.7 ms after loading. The jumping behaviour during unloading includes no high-frequency vibration component. Most of the vibration comprises low-frequency components. The author posits that the cause of sleeper-jumping is the abrupt release of the strain energy stored in the ballast.

Figure 9, as described, presents the vertical displacement of the sleeper. Presumably, similar behaviour occurs in the upper part of the ballast layer immediately under the sleepers, which means that the motion under impact loading is extremely slight. The compression and restoration behaviours are high-frequency responses that last for a very short time: about 1 ms. Therefore, high-frequency vibration components are dominant in ballast responses under loading. However, ballast motions during unloading are induced mainly by low-frequency vibration components that cause large displacement and which last longer.

6. Ballast layer modeling

Three-dimensional shape measurement was performed to ascertain three-dimensional vertex coordinates of more than 4000 ballast gravel pieces. Based on the measured coordinates, each shape was expressed using a polyhedral rigid-body discrete element model and was converted into aggregate, with the same size and the same shape, of the tetrahedron secondary elastic finite elements. Details of the measurements were presented in an earlier report [28]. **Figure 10** presents some exemplary images of a ballast gravel piece and its numerical discrete element and finite element models. Regarding the finite element models, a sufficiently fine

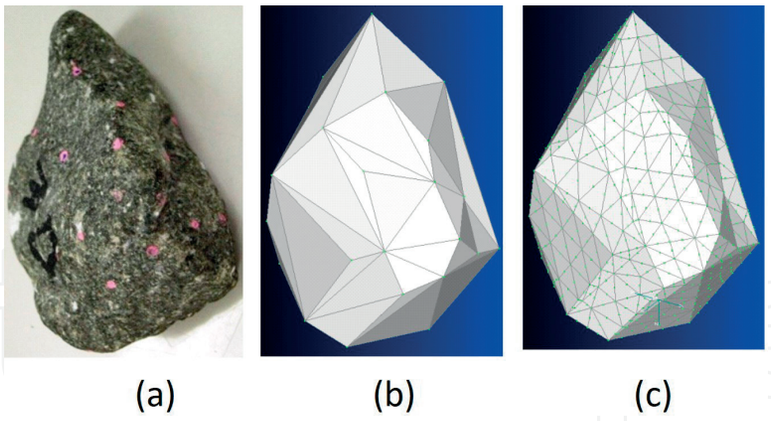


Figure 10. Exemplary pictures of existing ballasts and the digitized models. (a) Ballast, (b) DEM model, (c) FEM model.

mesh size of 1 cm was adopted to support the precise representation of natural frequencies of individual ballast gravel up to several 10 kHz.

Regarding the physical properties of the ballast, density ρ = 2700 (kg/m^3), Young's modulus E = 30 (GPa), Poisson's ratio ν = 0.2 and structural damping parameter η = 0.01 are adopted. The ballast gravel density was the laboratory experimental value obtained from specific gravity tests. The Young's moduli and Poisson's ratio were referred or derived from previous reports of the literature. Regarding the structural damping coefficient, the author adopted general values of a concrete structure.

Figure 11 presents a procedure for the creation of the ballast aggregate using both discrete element and finite element modeling. First, about 100 pieces of the ballast polyhedron discrete element models with different shapes and sizes were placed randomly in the air above rectangular box frames of 20 cm width and length. The gravel was then dropped freely with gravity and was compressed vertically with a loading plate using discrete element software. Next, all individual polyhedron discrete element models were converted into assemblages consisting of the small finite tetrahedron second-order elastic solid elements and split into 1 cm meshes with geometry and contact point information maintained. Each polyhedron discrete element model was divided into approximately 1000 tetrahedron finite elements. The finished rectangular block model has 20 cm width and length, with 17 cm height, and has more than 90,000 tetrahedron finite elements.

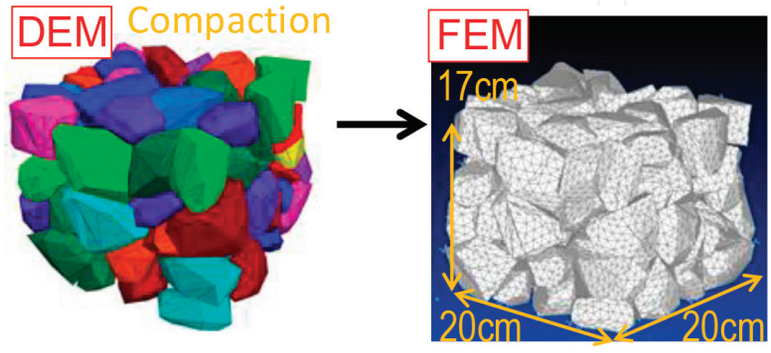


Figure 11. Compaction and modeling of the ballast aggregate with MPCs.

For this procedure, the contact points were mutually connected through multipoint constraints (MPCs), which connected the nodes of elements in three axial directions related to the contact pair of blocks at each contact point. The provided contact-connectivity exhibited no expansion or contraction because it was several tens of thousands of times harder than that of ballast pieces. Accordingly, the spring functions around the contact points were represented by the elastic deformation of the ballast angularities, which were composed of the assemblages of several tetrahedron finite elements adjacent to the contact points.

Figures 12 and **13** present a finite element model of a type 3 PC monoblock sleeper developed by the authors [24] and consisting of 51,146 nodes and 51,944 solid elements. The sleeper model can make a precise representation of all natural frequencies described above, with their response values up to 1 kHz within 5% deviation. Its physical weight is 161.40 kg. Its volume is 0.0677 m^3.

A large-scale finite element model was constructed with multipoint constraints (MPCs) by assembling 48 units of the rectangular unit block models of the ballast described above and

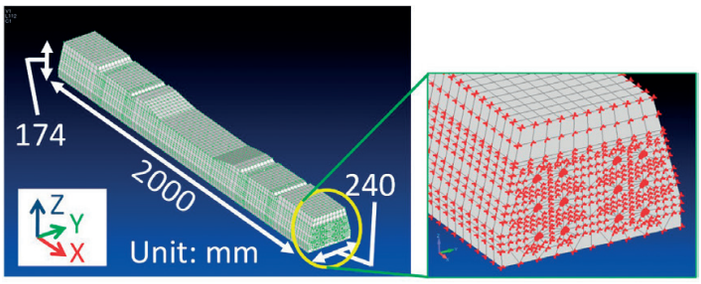


Figure 12. Model of a type 3 PC sleeper.

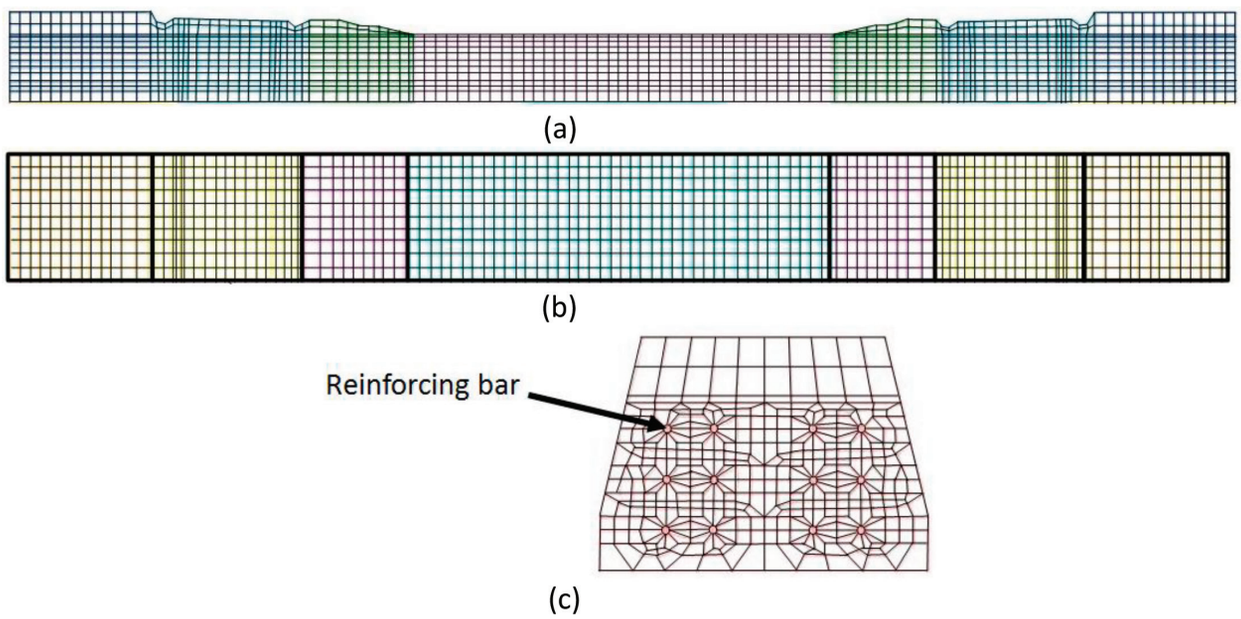


Figure 13. Model of a type 3 PC sleeper. (a) Side view, (b) top view, (c) end face and reinforce bars.

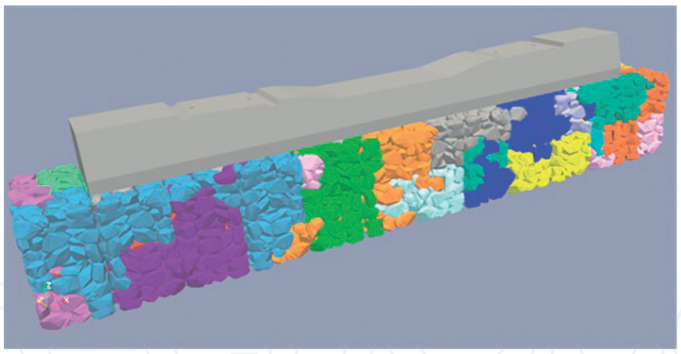


Figure 14. Assembly of ballasted track model and domain segmentation for large-scale parallel computing.

Item	Young's modulus (GPa)	Poisson's ratio	Density (kg/m^3)
Ballast	30	0.200	2700
Concrete	45	0.167	2350
Steel	210	0.290	7820

Table 1. Calculation parameters.

the type 3 PC sleeper model. **Figure 14** presents finished analysis model and its domain segmentation for large-scale parallel computing by the finite element programming code of FrontISTR. The model consists of 7.05 million nodes and 4.15 million second-order solid elements. The degrees of freedom of the model exceed 21 million. By adopting the finite element analysis using the precise model of the ballast layer having a complicated structure, it is possible to reproduce phenomena such as stress concentration and wave propagation within the ballast layer rapidly, easily and exactly. The entire model is divided into 24 sub-domains to introduce the direct solver MUMPS corresponding to the parallel computing of a distributed memory type. By applying the finite element normal-mode analysis by FrontISTR, a set of normal modes related to the ballast aggregate and sleeper system is obtained. Specifications related to the various parameters of each model are presented in **Table 1**.

7. Large-scale finite element transient response analysis of the elastic vibration mode of the ballasted track

The time history response waveforms were calculated numerically by inputting the measured loading waveforms to the top surface of a sleeper model when a passenger train moved over the top surface of the previously described ballasted track model.

Figure 15 displays the actual waveforms of vertical loading (measured in cross-sectional area of 14 cm width and 18 cm length on the bottom surface of the rails) applied by the first axles of a lead coach bogie when the passenger train moved through the test section at about 120 km/h [26, 27].

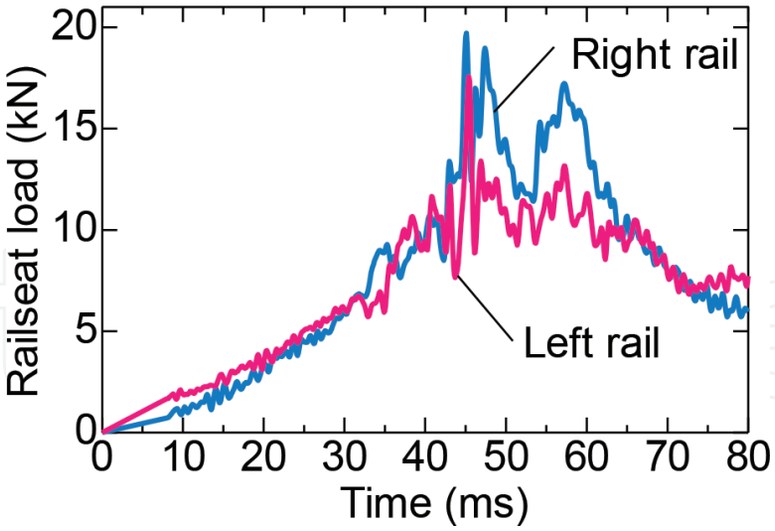


Figure 15. Measured rail seat loads.

The figure shows that the axles passed immediately above the sleeper centre at around 55 ms. Finite element analysis shows that the measured time history waveforms are uniformly input to all nodal points located within the bottom area of the rails on the top surface of the sleeper model. The calculation time interval is set at $\Delta t = 0.1$ (ms). The total calculation steps are 800.

Figure 16 portrays the distribution of the response nodal displacement of the ballast aggregate and the sleeper system at $t = 55.0$ (ms) when the load peaks appeared as the first axle of the lead coach bogie that passed above the sleeper centre. It is apparent that the dynamic displacement induced by a passing train on the ballast is not distributed uniformly throughout the ballast aggregate and the sleeper. Significant displacement is concentrated locally around the rail positions. Analytical results demonstrate that 30 μm maximum downward displacement occurred.

Figure 17 depicts the time history waveforms of response of the von Mises stress on the cross-section inside the gravel angle acting on three contact points, each with some angularity, of the ballast gravel placed at different depths below the loading point of the left rail location. As the figure shows, the stresses in the gravel increase gradually, alternately repeating the minute

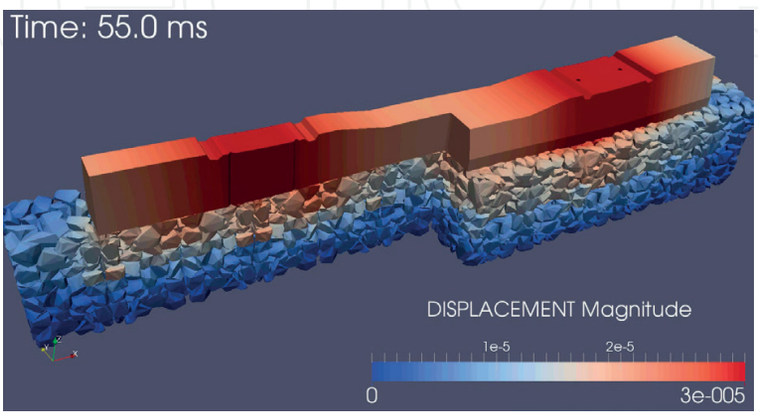


Figure 16. Distribution of nodal displacement ($t = 55.0$ ms).

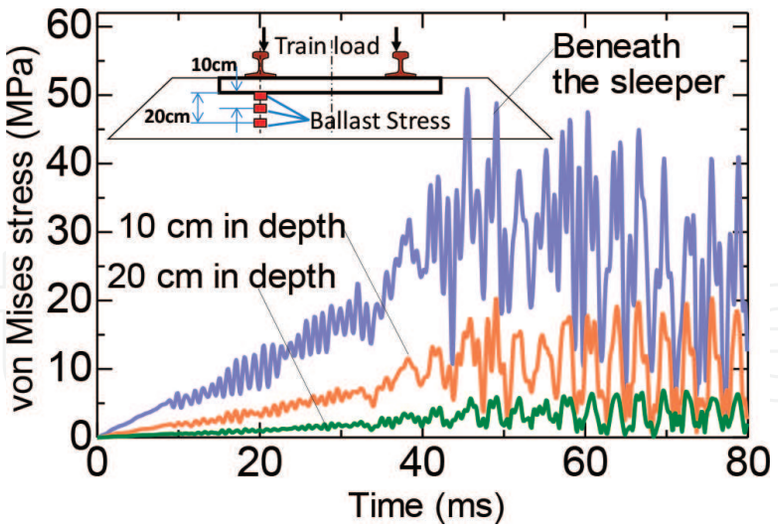


Figure 17. Time history of on Mises stress.

upward (compression) and downward (tension) motions at a frequency of approximately 300 Hz, according to the inputted loads. In this case, the maximum stresses of approximately 50 MPa after elapsed time of about 45–53 ms are observed near the ballast surface beneath the sleeper bottom. It is apparent that the rise in the peak response value becomes gentler as the measurement point becomes increasingly distant (i.e. deeper) from the loading point. A tendency exists for waveforms to become smoother along with the steep decrease in high-frequency vibration included in the wave. Although the investigation reported here involves elastic body analysis without the use of any constitutive equation, the diminishing trend of energy inside the ballast is reproduced closely by simulating the ballast aggregate structure in detail. Results show that the ballast aggregate structure featuring angular parts has the mechanism of energy attenuation.

Figure 18 portrays linear amplitude spectra of response of the von Mises stress on the cross-section inside the gravel angle acting at different depths below the loading point of the left rail, as obtained by conducting fast Fourier transformation of these time history response waveforms and smoothing them at a 20 Hz bandwidth. As the figure shows, these spectra curves identify the first-order elastic vibration resonance mode of the ballast layer at around 337 Hz, where the whole ballast layer stretches vertically as an elastic body.

To detect the exact frequency of the elastic vibration mode of the ballast layer, the author conducted a numerical experiment (simulation), which simulates the impulse loading experiment using a transient response analysis of the previously described large-scale sleeper-ballast aggregate model.

Figure 19 shows the amplitude spectra of response of the vertical displacement of the sleeper by application of a 0.1 ms square waveform of impulse loading. Impulse loading to the left and right rails totals 100 kN. Results of the numerical experiment of the impact loading indicate that the rigid-body natural vibration mode occurs at around 310 Hz. Results show that the analytical natural frequency of the elastic vibration mode of the ballast layer more or less coincides with the measured one described above and that the frequency corresponds to three times the value of the measured natural frequency of the rigid-body mode.

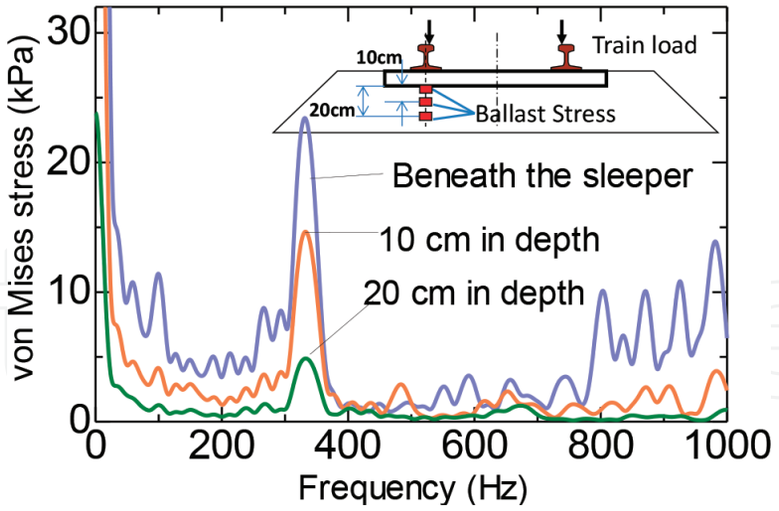


Figure 18. Response spectrum of the von Mises stress.

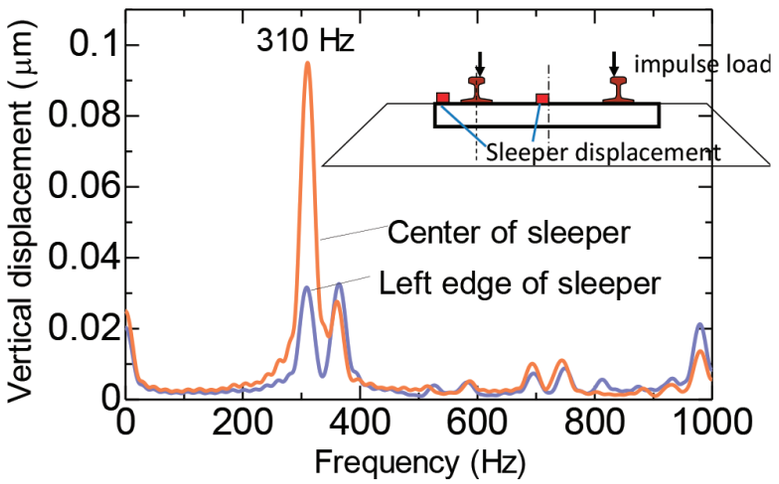


Figure 19. Response spectrum of vertical displacement regarding impulse loading.

8. Large-scale finite element transient response analysis related to the rigid-body vibration mode of the ballasted track

To examine the dominant rigid-body resonance motion around 100 Hz, this chapter presents a description of the large-scale finite element transient response analysis of the ballasted track using nonlinear contact springs (i.e. tensionless springs) in place of the MPCs. Results of the drop-weight tests described above suggest that the jumping motion of the ballasted track, the rigid-body bounce mode, will cause large displacement. Therefore, regarding the previously described large-scale finite element model of the ballasted track, information of the contact points between the ballast pieces and the sleeper nodes is modeled with nonlinear contact springs, that is, with tensionless contact. **Table 2** presents parameters of calculations related to contact points. In this analysis, the tension spring factors are set at 1/100,000 values of the compression spring factors.

Item	Compression spring factor (GN/m)	Tension spring factor (GN/m)
Ballast-ballast	30	0.0003
Sleeper-ballast	10	0.0001

Table 2. Calculation parameters related to contact points.

With finite element analysis, the measured waveforms of the rail seat load were inputted to the top surface of the sleeper model using tensionless springs. **Figure 20** presents the nodal displacement distribution of the ballast aggregate and the sleeper system at t = 55.0 ms when load peaks appeared immediately after the first axle of the lead coach bogie passed above the sleeper centre.

Figure 21 depicts time history waveforms of the response of the von Mises stress on the cross-section inside the angular part of the gravel under the left rail. As the figure shows,

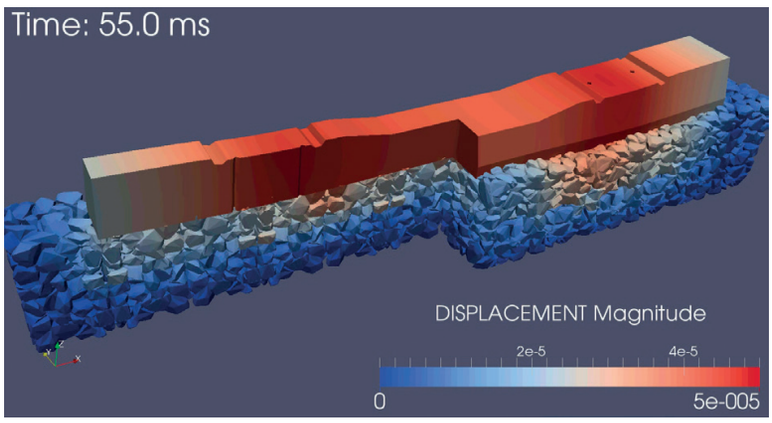


Figure 20. Distribution of nodal displacement (t = 55.0 ms).

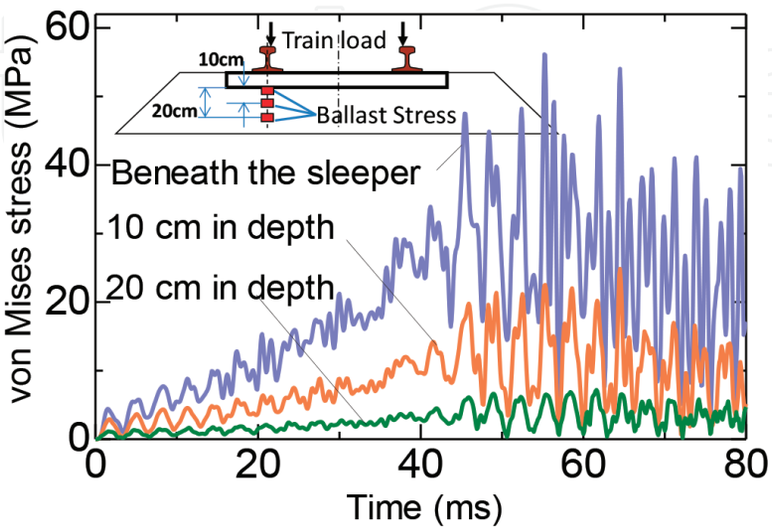


Figure 21. Time history response of the von Mises stress.

considerable stresses of approximately 57 MPa are obtained near the surface of the ballast layer under the sleeper bottom. In the figure, in general, the positive motion denotes compression and downward behaviour. Negative motion denotes tension and upward behaviour.

Figure 22 displays the linear amplitude spectra of response of von Mises stress, on the cross-section inside the gravel angle acting at different depths below the loading point of the left rail, which are obtained by conducting fast Fourier transformation of these time history response waveforms and by smoothing them at 20 Hz bandwidth. As the figure shows, these spectral curves identify the first-order elastic vibration resonance mode of the ballast layer at around 337 Hz, where the entire ballast layer stretches vertically as an elastic body.

Figure 23 presents the time history of response of the vertical displacement at the left edge of the sleeper immediately after the 0.1 ms square impulse loading waveforms of 100 kN. In this figure, the downward displacement shows the downward motion of the sleeper (i.e. ballast

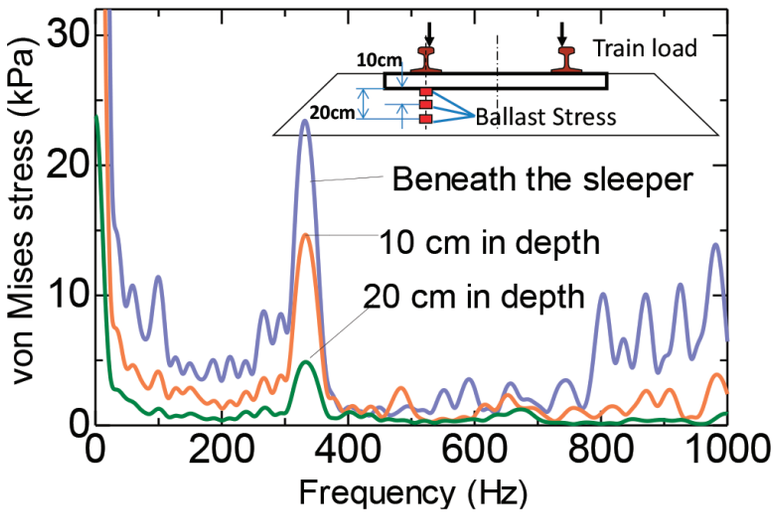


Figure 22. Spectra of von Mises stress.

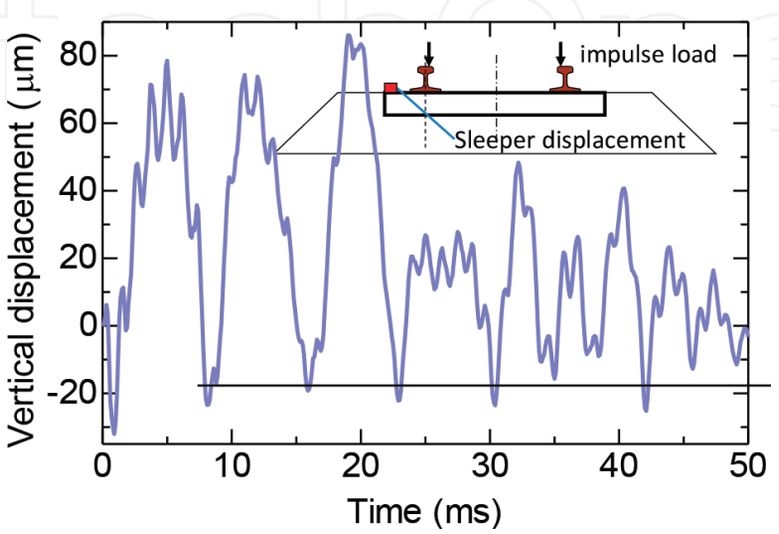


Figure 23. Time history response of sleeper displacement.

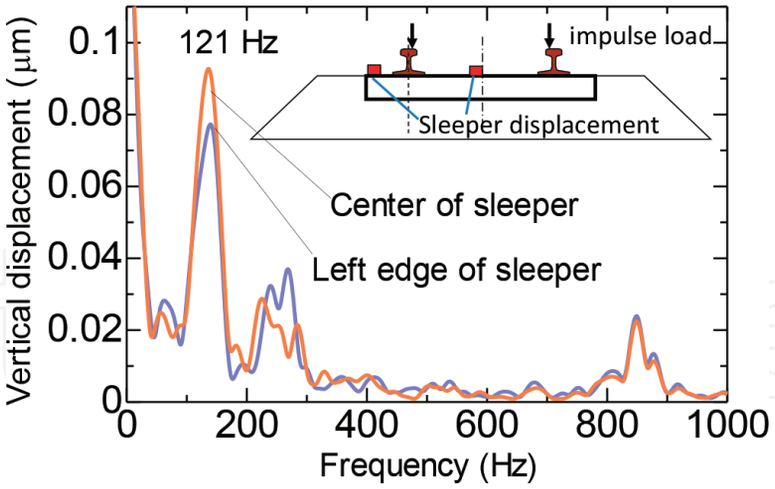


Figure 24. Response spectrum of vertical displacement related to impulse loading.

layer compression); the upward displacement represents the upward motion of sleeper (i.e. ballast layer extension). According to the figure, when an impact load is applied, the ballast layer instantaneously deforms elastically because of compression. It then returns to the pre-loading position. Consequently, it takes only about 1 ms for the ballast layer to be compressed and restored. Following compression and restoration of the ballast layer, sleeper-jumping occurs. The cause of this sleeper-jumping is the strain energy stored in the ballast under the compression procedure and its abrupt release.

Figure 24 presents amplitude spectra of the vertical displacement of the sleeper. Results indicate that rigid-body natural vibration occurs at around 120 Hz. The value is approximately 10–20% larger than the experimental one and is almost one-third of the elastic natural vibration frequency. Large-scale finite element analysis by tensionless analysis reveals that rigid-body natural vibration mode occurs at almost one-third of the elastic natural vibration frequency.

9. Stress on the cross-section inside the angular part of the gravel

Figure 25 presents time history waveforms of response of the von Mises stress on the cross-section inside the angular part of the gravel where the maximum response stress occurs. This analysis shows that strong stresses up to 80 MPa can be observed in tetrahedral elements near the contact part, whereas the average maximum pressure on the ballast surface is 74 kPa. The stress acting on the angular part is approximately 1100 times greater than the average value of the loading stress on the ballast surface. Assuming that the unconfined compressive strength is 60 MPa at the angular part of the ballast gravel, the application of a dynamic load of 55 kPa or more to the surface of the ballast layer under the bottom surface of the sleeper would cause minute fracturing or breakage around the angular part of the ballast gravel, where the stress will converge.

Figure 26 presents results of measurements indicating the maximum values for all sensors (measured in a cross-sectional square area with 8 cm sides on the whole bottom surface of the sleeper, total: 75 pieces, 25 units × 3 rows) as the passenger train passed. The figure also shows a threshold line of 55 kPa at which breakage will occur in the angular part of the ballast gravel.

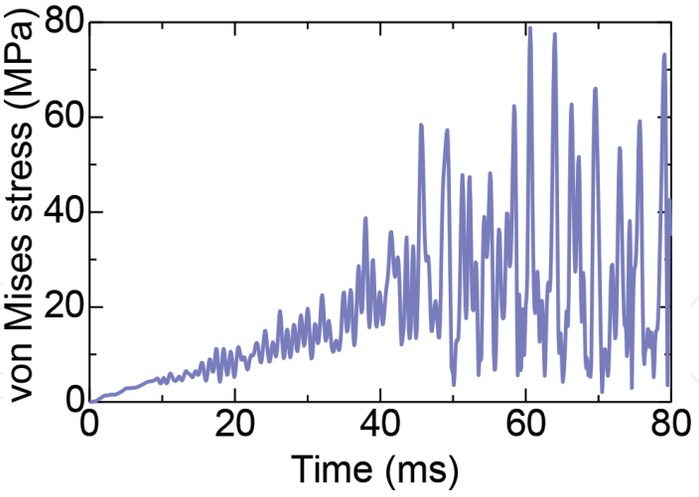


Figure 25. Time history response waveforms of the von Mises stress.

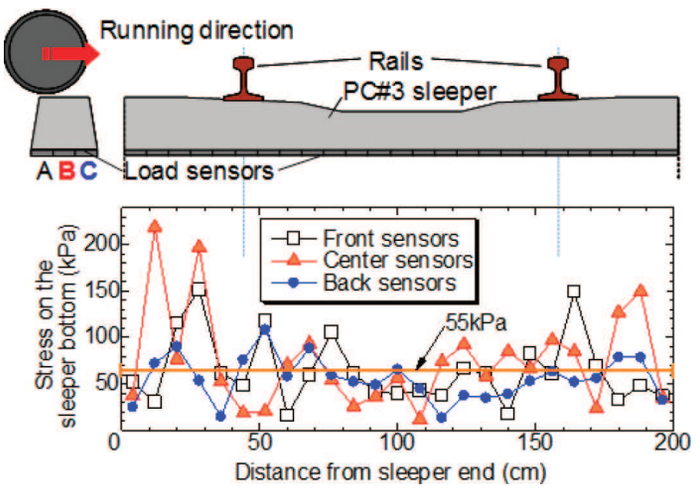


Figure 26. Distribution of the maximum load acting during passage of a passenger train.

Minute breakage might occur at points within the ballast layer where the stress converges if the measured value exceeds this line. As the figure shows, this limit was exceeded in 40 out of the 75 sensors; the ratio of exceeding the threshold is 53%. The results indicate that the degradation of the ballast layer might occur at any time under the effects of regular train passage. Further experimentation and analysis must be conducted to clarify this issue.

10. Relations among natural vibration modes of ballasted track

According to the results, when information related to the contact points between the sleeper bottom and ballast pieces is modeled with MPCs, numerically obtained results show that the vertical elastic natural vibration mode of the ballast layer occurred at about 310 Hz. However, when the contact point is modeled with nonlinear contact springs, i.e. with tensionless contact, the rigid-body natural vibration mode is found numerically as approximately 120 Hz.

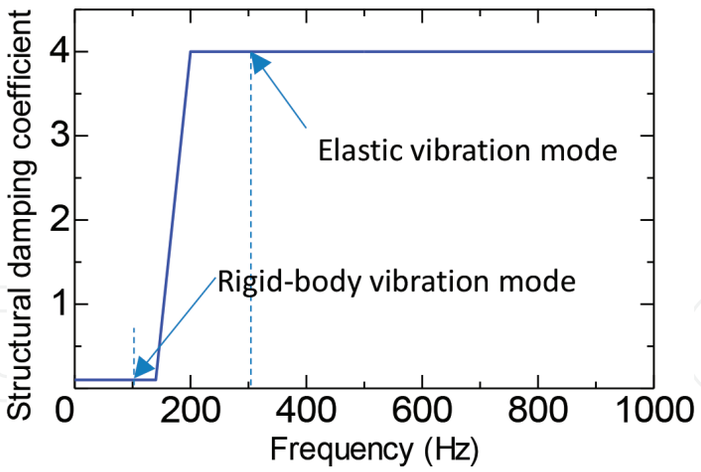


Figure 27. Structural damping coefficient in the vertical direction for a 30 cm-thick ballast layer.

The analytical result coincides to a considerable degree with those obtained using in situ measurements and full-scale experiments. Accordingly, the natural mode which is expected to occur when an impact load is applied is determined mainly by the contact condition on the sleeper bottom.

As shown in **Figure 5** presented earlier, the amplitude of displacement of the ballast gravel decreases in inverse proportion to the squares of the frequency, according to the physical theory. Therefore, the occurrence of the rigid-body natural vibration at one-third of the elastic natural vibration frequency is expected to induce nine times larger amplitude of displacement within the composite structure of the ballasted track than in the case of the elastic natural frequency. The occurrence of the rigid-body natural vibration is expected to contribute greatly to the progress of the ballast deterioration. In theory, improvement of the contact condition between the sleeper bottom and the boundary region of the ballast layer might reduce the amplitude of displacement to one-ninth at most compared with that in the current status of the ballasted track. Moreover, measurements of the ratio of the rigid-body natural vibration and the elastic vibration at the site are expected to contribute to quantitative evaluation of the ballasted track condition.

Figure 27 presents the structural damping coefficient on the sleeper bottom in the vertical direction for a 30 cm-thick ballast layer, as identified by the experimental model analysis using full-scale mock-ups of the ballasted track and precise finite element analysis according to an earlier report of the literature [24]. As the figure shows, the structural damping factor of the ballasted layer has extremely strong dependence on the frequency. The ballast layer, in the high-frequency domain over 200 Hz, provides extremely high damping functions for reducing the impact energy. However, the ballast layer is almost non-resistant to the wave components of dynamic loads in the low-frequency domain. The load components in the low-frequency domain will be reduced only slightly unless the ballast aggregate is fully constrained by an appropriate amount of uniform pressure from the surrounding area. To reduce the ballast degradation based on these mechanisms, improvement of the contact condition of the boundary region adjacent to the sleeper bottom in the ballast layer contributes to restraint of the occurrence of the rigid-body natural vibration modes at low frequencies.

11. Conclusions

As described in this chapter, although the results are limited to the ballasted track of metre-gauge railway lines in Japan, the author dealt with natural vibration modes of the ballast layer, which will engender the phenomena of ballast deterioration, based on precise field measurement, full-scale experiments and large-scale numerical analyses based on high-performance parallel computing. These results can be summarized as described below.

1. Impact loads imposed by running trains induce natural vibration modes within the ballast layer that are specific to the structure and which consequently propagate within the ballast layer through the natural vibration modes. Natural vibration modes play an important role in ballast layer deterioration.
2. According to drop-weight impact loading test, the high-frequency vibration components are dominant in the ballast responses under loading. The ballast motions during unloading are induced mainly by low-frequency vibration components that cause large displacement and which last longer.
3. Analytical results indicate that the stress acting on the angular part of the ballast gravel is approximately 1100 times greater than the average loading stress on the ballast surface under the sleeper bottom. Minute fracturing or breakage around locations where the stress acting on the angular part of the ballast gravel converges will occur at any time because of the effects of regular train passage.
4. Normal frequencies of the vertical elastic vibration mode are detected numerically at around 310 Hz. The rigid-body bounce mode of the ballast layer occurs at almost one-third of the frequency of the elastic vibration mode. These analytical normal frequencies coincide closely with the measured ones.
5. The occurrence of rigid-body modes of the ballast layers plays an important role in the progress of ballast deterioration. The improvement of the contact condition near the sleeper bottom is expected to contribute to reduction of the displacement amplitude of ballast gravel. That will reduce the ballast degradation.
6. The combined structure, which consists of the ballast layer and sleepers, vibrates in synchrony with resonance motions induced by the impulse waves. Improvement of contact conditions near the sleeper bottom is expected to contribute to reduce the displacement amplitude of the ballast gravel and to reduce ballast degradation.

Author details

Akira Aikawa

Address all correspondence to: aikawa.akira.11@rtri.or.jp

Track Dynamics Laboratory, Railway Dynamics Division, Railway Technical Research Institute, Tokyo, Japan

References

[1] Kaewunruen S, Remennikov AM. Sensitivity analysis of free vibration characteristics of an in situ railway concrete sleeper to variations of rail pad parameters. Journal of Sound and Vibration. Nov 2006;**298**(1-2):453-461

[2] Kaewunruen S, Aikawa A, Remennikov AM. Vibration attenuation at rail joints through under sleeper pads. Procedia Engineering. May 2017;**189**:193-198

[3] Sol-Sánchez M, Moreno-Navarro F, Rubio-Gámez MC. The use of elastic elements in railway tracks: A state of the art review. Construction and Building Materials. Jan 2015; **75**:293-305

[4] Remennikov A, Kaewunruen S. Experimental investigation on dynamic railway sleeper/ ballast interaction. Experimental Mechanics. Feb 2006;**46**(1):57-66

[5] Kaewunruen S, Ishida M, Marich S. Dynamic wheel–rail interaction over rail squat defects. Acoust Australia. Mar 2015;**43**(1):97-107

[6] Zhao X, Li Z. The solution of frictional wheel-rail rolling contact with a 3D transient finite element model: Validation and error analysis. Wear. May 2011;**271**(1-2):444-452

[7] Zhao X, Zhao X, Liu C, Wen Z, Jin X. A study on dynamic stress intensity factors of rail cracks at high speeds by a 3D explicit finite element model of rolling contact. Wear. Nov 2016;**366-367**:60-70

[8] Sakai H, Takagaki M, Hayashi M, Aikawa A. Analysis of rolling contact behavior between wheel and rail through large-scale parallel computing. Quarterly Report of RTRI. Oct 2014;**55**(3):171-175. Available from: www.jstage.jst.go.jp/browse/rtriqr/55/3/_ contents/-char/en

[9] Aikawa A. Research on vertical natural vibration characteristics of gravel aggregate in ballasted track. Quarterly Report of RTRI. 2015;**56**(1):26-32. Available from: www.jstage. jst.go.jp/article/rtriqr/56/1/56_26/_article/-char/en [Accessed: March 16, 2015]

[10] Aikawa A, Techniques to measure effects of passing trains on dynamic pressure applied to sleeper bottoms and dynamic behavior of ballast stones. Quarterly Report of RTRI. 2009;**50**(2):102-109. Available from: www.jstage.jst.go.jp/article/rtriqr/50/2/50_2_102/_ article/-char/en [Accessed: June 2, 2009]

[11] Aikawa A. Determination of dynamic ballast characteristics under transient impact loading. Electronic Journal of Structural Engineering (Special Issue—Advances in Rail Track Infrastructure Research and Practice (ARTIRP)-2013). Apr 2014:17-34

[12] Aikawa A. Dynamic characterisation of a ballast layer subject to traffic impact loads using three-dimensional sensing stones and a special sensing sleeper. Construction and Building Materials. 2015;**92**(1):23-30

[13] Aikawa A. Impact-loading-test regarding ballast subsidence countermeasures using high-damping under sleeper pads and high-strength artificial ballast cubes. In: Forde MC, editor. Railway Engineering. ECS Publications, Edinburgh, UK. 2017. ISBN: 0-947644-83-014

[14] CERFACS, ENS Lyon, INPT (ENSEEIHT)-IRIT, Inria and University of Bordeaux. Multifrontal Massively Parallel Solver (MUMPS 5.1.2) Users' Guide. Oct 2017;94. Available from: http://graal.ens-lyon.fr/MUMPS/

[15] Amestoy PR, Duff IS, L'Excellent J-Y. Multifrontal parallel distributed symmetric and unsymmetric solvers. Computer Methods in Applied Mechanics and Engineering. 2000;**184**:501-520

[16] Amestoy PR, Duff IS, Koster J, L'Excellent J-Y. A fully asynchronous multifrontal solver using distributed dynamic scheduling. SIAM Journal of Matrix Analysis and Applications. 2001;**23**(1):15-41

[17] Amestoy PR, Guermouche A, L'Excellent J-Y, Pralet S. Hybrid scheduling for the parallel solution of linear systems. Parallel Computing. 2006;**32**(2):136-156

[18] Okuda H. FrontISTR Ver4.5 User's Manual, Research and Development for Next-generation Information Technology of Ministry of Education, Culture, Sports, Science and Technology, "Research and Development of Innovative Simulation Software," FrontISTR Commons. July 2016. Available from: http://www.frontistr.org/

[19] Yuan X. Advance/FrontSTR. Advance Simulation. Dec 2016;**23**:50-54. AdvanceSoft Corporation. Available from: http://www.advancesoft.jp/ (in Japanese)

[20] Aikawa A. Finite element transient response analysis on the vertical natural vibration modes of the combined structure of the ballast layer and a sleeper. Journal of Japan Society of Civil Engineers, Ser. A2 (Applied Mechanics (AM)). 2015;**71**(2):I_125-I_136. Feb 2016 (in Japanese)

[21] Grassie SL, Gregory RW, Harrison D, Johnson KL. Modelling of railway track and vehicle/track interaction at high frequencies. Vehicle System Dynamics. 1993;**22**(3-4):209-262

[22] Aikawa A. Application of a special sensing sleeper for dynamic interaction within the boundary layer between a sleeper and ballasts. In: The 11th International Conference on Computational Structures Technology (CST2012), Paper No. 130, Dubrovnik, Croatia: Civil-Comp Press, Stirlingshire, Scotland, UK; 2012. ISBN: 978-1-905088-54-6

[23] Aikawa A, Urakawa F, Abe K, Namura A. Dynamic characteristics of railway concrete sleepers using impact excitation techniques and model analysis. In: The Ninth World Congress on Railway Research (WCRR). Lille, France: SNCF; May 22-26, 2011

[24] Sakai H, Aikawa A. Finite element vibration analysis of sleepers including ballast damping characteristics. International Journal of Railway Technology (IJRT). 2012;**1**(3):37-59

[25] Railway Bureau, MILT (Ministry of Land, Infrastructure, Transport and Tourism, and Railway Technical Research Institute, Japan) and RTRI. Design Standards for Railway Structures and Commentary (Track Structures). Maruzen Publishing Co. Ltd; Kanda Jimbo-cho, Chiyoda-ku, Tokyo, Japan; 2012 (in Japanese)

[26] Urakawa F, Aikawa A, Namura A, Kono A. Development of remote automatic measuring system for long-term measurement of dynamic responses of tracks. Proceedings of Railway Mechanics. 2009;**13**:23-28 (in Japanese)

[27] Aikawa A, Urakawa F, Kono A, Namura A. Sensing sleeper for dynamic pressure measurement on a sleeper bottom induced by running trains. In: Railway Engineering. In: Forde MC, editor. UK: University of Edinburgh, Railway Gazette International; 2009. ISBN: 0-947644-65-2

[28] Aikawa A. DEM modeling techniques for dynamic analysis of ballasted railway track. In: 2nd International FLAC/DEM Symposium. Melbourne, Australia: ITASCA; 2011

IntechOpen

IntechOpen

IntechOpen

IntechOpen